

International Journal of Modern Physics A  
 © World Scientific Publishing Company

## Study of the cosmogenic activation in NaI(Tl) crystals within the ANAIS experiment

P. Villar,\* J. Amaré, S. Cebrián, I. Coarasa, E. García, M. Martínez,† M. A. Oliván, Y. Ortigoza, A. Ortiz de Solórzano, J. Puimedón, M. L. Sarsa and J. A. Villar ‡

*Laboratorio de Física Nuclear y Astropartículas, Universidad de Zaragoza,  
 C/Pedro Cerbuna 12, 50009 Zaragoza, Spain*

*Laboratorio Subterráneo de Canfranc,  
 Paseo de los Ayerbe s.n., 22880 Canfranc Estación, Huesca, Spain  
 \*pvillar@unizar.es*

Received Day Month Year  
 Revised Day Month Year

The direct detection of galactic dark matter particles requires ultra-low background conditions. NaI(Tl) crystals are applied in the search for these dark matter particles through their interactions in the detector by measuring the scintillation signal produced. The production of long-lived isotopes in materials due to the exposure to cosmic rays on Earth's surface can be a hazard for these ultra-low background demanding experiments, typically performed underground. Therefore, production rates of cosmogenic isotopes in all the materials present in the experimental set-up, as well as the corresponding cosmic rays exposure history, must be both well known in order to assess the relevance of this effect in the achievable sensitivity of a given experiment.

Here, analysis of the cosmogenic studies developed from the ANAIS experiment NaI(Tl) detectors are presented. Installed inside a convenient shielding at the Canfranc Underground Laboratory just after finishing surface exposure to cosmic rays and thanks to the prompt data taking developed, identification and quantification of isotopes with half-lives of the order of tens of days were allowed, and thanks to the long-term operation of the detectors long-lived isotopes have been also identified and quantified. Main results for the activation yields of iodine and tellurium isotopes,  $^{22}\text{Na}$ ,  $^{113}\text{Sn}$ ,  $^{109}\text{Cd}$ , and tritium are presented in this work, together with the estimate of the production rates for their activation by cosmic nucleons while on Earth's surface based on a selection of excitation functions over the entire energy range of cosmic nucleons.

*Keywords:* Cosmogenic activation; cosmic-rays; dark matter; NaI detectors; radionuclide.

29.40.Mc, 95.35.+d, 13.85.Tp, 25.40.-h:

\*Corresponding author

†Present Address: Università di Roma La Sapienza, Piazzale Aldo Moro 5, 00185 Roma, Italy.

‡Deceased

## 1. Introduction

Sodium iodide crystals (Tl doped) have been widely used as radiation detectors profiting from the very high light output. In particular, NaI(Tl) detectors have been applied in the direct search for dark matter (the so-called WIMPs, which could be filling the galactic dark matter halo) for a long time. Among the several experimental approaches using NaI(Tl) detectors, DAMA/LIBRA is the most relevant, having reported the observation of a modulation compatible with that expected for galactic halo dark matter particles with a large statistical significance.<sup>1</sup> Results obtained with other target materials and detection techniques have been ruling out for years the most plausible compatibility scenarios. The ANAIS (Annual modulation with NaI Scintillators) project<sup>2</sup> is searching for dark matter annual modulation with 112.5 kg of ultrapure NaI(Tl) scintillators since August 2017 at the Canfranc Underground Laboratory (LSC) in Spain; the aim is to provide a model-independent confirmation of the annual modulation positive signal reported by DAMA/LIBRA using the same target and technique.<sup>3</sup>

Production of long-lived radioactive isotopes due to exposure to cosmic rays<sup>4-7</sup> is a well-known sensitivity limiting hazard for experiments aiming at the detection of rare events, in particular, for experiments searching for the nuclear double beta decay or the interaction of WIMPs, requiring detectors working in ultra-low background conditions. Operating in deep underground locations, using active and passive shields and selecting carefully radiopure materials are common practices in these experiments in order to reduce very efficiently the background entangling the searched signal.<sup>8,9</sup> Cosmogenic radionuclides produced during fabrication, transport and storage of components may be even more important than residual contamination from primordial nuclides and become very problematic. For instance, the poor knowledge of cosmic ray activation in detector materials is highlighted<sup>10</sup> as one of the three main uncertain nuclear physics aspects of relevance in the direct detection approach pursued to solve the dark matter problem.

In principle, cosmogenic activation can be kept under control by minimizing exposure at surface and storing materials underground, avoiding flights and even using shields against the hadronic component of cosmic rays while surface building and operation of the detector. But since these requirements usually complicate the preparation of experiments (for example, while crystal growth and detector mounting steps) it would be desirable to have reliable tools to quantify the real danger of exposing the different materials to cosmic rays. Direct measurements, by screening of exposed materials in very low background conditions as those achieved in underground laboratories, and calculations of production rates and yields, following different approaches, have been made for several materials in the context of dark matter, double beta decay and neutrino experiments. Many different studies are available for germanium and interesting results have been derived in the last ye-

ars<sup>6,11</sup> also for other detector media like tellurium and TeO<sub>2</sub>,<sup>12–14</sup> xenon<sup>15,16</sup> or neodymium,<sup>17,18</sup> as well as for materials commonly used in the set-ups like copper,<sup>15,16,19–21</sup> lead,<sup>22</sup> stainless steel,<sup>16,20</sup> titanium<sup>16</sup> or teflon.<sup>16</sup>

In general, relevant long-lived radioactive isotopes cosmogenically induced are different for each target material. However, there are some common dangerous products like tritium, generated in any material due to its spallation product nature. Tritium is specially worrisome for dark matter experiments due to its decay properties (it is a pure beta emitter with transition energy of 18.591 keV and a long half-life of 12.312 y<sup>23</sup>) when induced in the detector medium. Moreover, quantification of tritium cosmogenic production is not easy, neither experimentally (since its beta emissions are hard to disentangle from other background contributions) nor by calculations (as tritium can be produced by different reaction channels).

Estimates of activation yields in NaI(Tl) corresponding to long-lived radioactive isotopes relevant in the frame of rare events experiments are presented here. These estimates take into consideration both measurements and calculations. NaI(Tl) has been used for dark matter searches for a long time<sup>24–32</sup> and only very recently activation yields in this material have been quantified.<sup>33,34</sup> Here, measurements and calculations correspond to ANAIS data from nine 12.5 kg NaI(Tl) detectors which were installed inside a convenient shielding at the LSC, just after finishing surface exposure to cosmic rays during production. The very fast start of data taking for all modules allowed to identify and quantify isotopes with half-lives of the order of tens of days. Also, the presence of long-lived isotopes has been possible by analyzing data taken after a few months underground.

Successful background models have been built for different ANAIS detectors.<sup>35,36</sup> First, we considered contributions to the background from those isotopes identified and quantified by the usual radiopurity measurements. However, to reproduce the measured data, additional contributions have to be included into the model. In this work we address the cosmogenic contribution.<sup>33</sup> Production of iodine and tellurium isotopes, <sup>113</sup>Sn, <sup>109</sup>Cd, <sup>22</sup>Na and <sup>3</sup>H in NaI(Tl) crystals has been observed in the ANAIS detectors and is analysed in the following sections.

The structure of this paper is the following: section 2 describes the evolution and experimental set-ups of the ANAIS experiment including electronics and data analysis. Section 3 presents activation results for different isotopes in the NaI(Tl) crystals, including production rates at sea level derived for most of the identified radionuclides considering the history of the detectors. A calculation of the corresponding production rates has been also attempted using carefully selected excitation functions, as shown in section 4. In section 5, a comparison between activation results derived from ANAIS and other experiments is made. Finally, a brief summary

4 *P. Villar et al.*

is presented in section 6.

## 2. The ANAIS experiment

ANAIS-112 experiment uses nine NaI(Tl) modules produced by Alpha Spectra Inc. (AS) in Colorado. These modules have been manufactured along several years and then shipped to Spain, avoiding air travel, arriving at LSC the first of them at the end of 2012 and the last one by March, 2017 (see Table 1). Each crystal is cylindrical (4.75" diameter and 11.75" length), with a mass of 12.5 kg. NaI(Tl) crystals were grown from selected ultrapure NaI powder and housed in OFE (Oxygen Free Electronic) copper; the encapsulation has a mylar window allowing low energy calibration. Two Hamamatsu R12669SEL2 photomultipliers (PMTs) were coupled through quartz windows to each crystal at LSC clean room. All PMTs have been screened for radiopurity using germanium detectors in Canfranc. The shielding for the experiment consists of 10 cm of archaeological lead, 20 cm of low activity lead, 40 cm of neutron moderator, an anti-radon box (continuously flushed with radon-free air) and an active muon veto system made up of plastic scintillators designed to cover top and sides of the whole ANAIS set-up (see Fig. 1). The hut housing the experiment is at the hall B of LSC under 2450 m.w.e.

Before the full installation of ANAIS-112 set-up, the first modules received at Canfranc were operated in a different set-up, very similar to that of the final experiment, allowing for a long and stable data taking. Protocols for data acquisition and analysis have been the same from the very beginning.

ANAIS-25 modules (D0 and D1) arrived at LSC in the evening of 27<sup>th</sup> November 2012 and were immediately stored underground; data taking started only three days later, after coupling PMTs in the LSC clean room, placing the detectors inside the shielding and testing of electrical connections and general performance. ANAIS-25

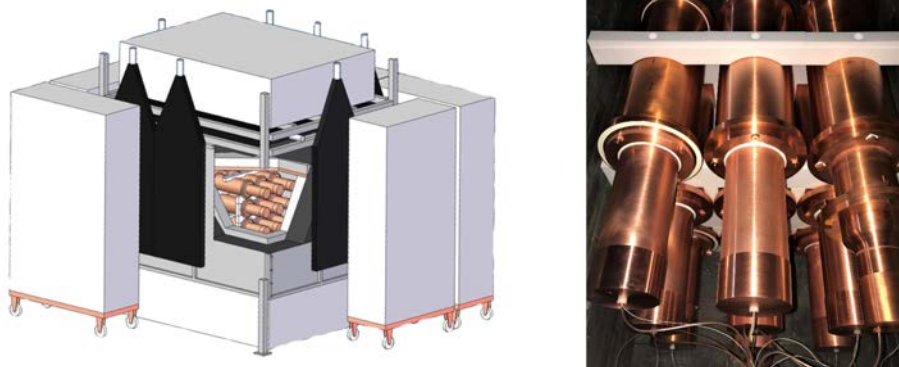


Fig. 1. Schematic view of the ANAIS-112 set-up (left) and picture of the inside (right).

Table 1. Features of the nine ANAIS detectors produced by Alpha Spectra: type of NaI(Tl) powder used, date of arrival at LSC and light collection.

Detector	Quality powder	Arrival date	Light collection (phe/keV)
D0	<90 ppb K	December 2012	$15.3 \pm 1.1$
D1	<90 ppb K	December 2012	$14.8 \pm 0.5$
D2	WIMP-Scint-II	March 2015	$15.3 \pm 1.4$
D3	WIMP-Scint-III	March 2016	$14.6 \pm 0.8$
D4	WIMP-Scint-III	November 2016	$14.0 \pm 0.8$
D5	WIMP-Scint-III	November 2016	$14.0 \pm 0.8$
D6	WIMP-Scint-III	March 2017	$12.6 \pm 0.8$
D7	WIMP-Scint-III	March 2017	$17.0 \pm 2.0$
D8	WIMP-Scint-III	March 2017	$14.6 \pm 0.9$

set-up took data from December 2012 to March 2015.

The ANAIS-37, A37D3 and A37D5 set-ups were very similar. They consisted of three AS modules (D0-D2-D1, D0-D3-D2, and D3-D4-D5, respectively). Details on the arrival date and powder quality of these detectors are given in Table 1. The last three detectors (D6, D7 and D8) arrived on 15<sup>th</sup> March 2017 at LSC and were directly installed in the final set-up ANAIS-112. For all set-ups, the prompt commissioning allowed to observe short-lived isotopes and to properly quantify induced activation in those long-lived.

Concerning the data acquisition system, each PMT charge output signal is separately processed; each one is divided into a trigger signal, a signal going to the digitizer and several ones differently amplified/attenuated, and fed into QDC (charge-to-digital-converter) module channels to be integrated in a 1  $\mu$ s window. Triggering is done by the coincidence (logical AND) of the two PMT signals of any detector at photoelectron level in a 200 ns window, enabling digitization and conversion of the two signals. The building of the spectra is done by software (off-line) by adding the signals from the PMTs, and Pulse Shape Analysis is applied in order to select bulk scintillation events in the NaI crystals and to distinguish alpha interactions from beta/gamma ones.

Regarding the response of the detectors, it must be remarked the outstanding light collection measured for the nine AS modules at the level of  $\approx 15$  phe/keV<sup>37</sup> (see Table 1). This high light output has a direct impact in both resolution and energy threshold, but it also allows to improve strongly the signal vs noise filtering down to the threshold and hence, reduce analysis uncertainties in the search for dark matter annual modulation.

### 3. Activation results

Several cosmogenically induced isotopes have been identified in ANAIS NaI(Tl) crystals (see Table 2) thanks to different distinctive signatures (see Fig. 2). The initial specific activities measured when the detectors were moved underground have been determined and, in the case of iodine and tellurium isotopes and  $^{22}\text{Na}$ , an estimate of the production rates has been made from those specific activities. In the following, for brevity, we will refer to the specific activities as activities. Preliminary estimates of production rates of  $^{113}\text{Sn}$  and  $^{109}\text{Cd}$  are presented here too. For the different analyzed isotopes, their decay modes and relevance will be described, the methodology followed to quantify them discussed and the obtained results presented. When required, the detection efficiencies  $\epsilon$  have been obtained by Geant4 simulation taking into account the geometry of each set-up and considering isotopes homogeneously distributed in the crystals. This kind of Monte Carlo simulations was validated with a similar set-up, but slightly different detector geometry<sup>36</sup> by reproducing measurements with calibration sources.

Table 2. Main cosmogenically induced isotopes identified in the data of ANAIS modules. Half-lives and decay mechanisms are indicated. Fourth column shows the energy of analyzed signals: gamma emissions, excited levels of metastable states and binding energies of K-shell electrons for EC decays (see text). Last column gives the considered product of intensity  $I$  and detection efficiency  $\epsilon$  for the analyzed distinctive signal of each isotope (see text). Decay information for  $^{125}\text{I}$ ,  $^{127m}\text{Te}$ ,  $^{123m}\text{Te}$ ,  $^{113}\text{Sn}$ ,  $^{109}\text{Cd}$ ,  $^{22}\text{Na}$  and  $^3\text{H}$  has been taken from Ref. 38, for  $^{121m}\text{Te}$  from Ref. 39 and for the other isotopes from Ref. 40.

Isotope	Half-life	Decay mechanism	Main $\gamma$ emissions/ Metastable levels/ Electron binding energy (keV)	$I\epsilon$
$^{126}\text{I}$	$(12.93 \pm 0.05)$ d	EC, $\beta^+$ , $\beta^-$	666.3	0.0035
$^{125}\text{I}$	$(59.407 \pm 0.009)$ d	EC	35.5 (+ 31.8)	0.8011
$^{127m}\text{Te}$	$(106.1 \pm 0.7)$ d	IT, $\beta^-$	88.3	0.9727
$^{125m}\text{Te}$	$(57.4 \pm 0.2)$ d	IT	144.8	0.968
$^{123m}\text{Te}$	$(119.3 \pm 0.2)$ d	IT	247.6	0.972
$^{121m}\text{Te}$	$(164.2 \pm 0.8)$ d	IT, EC	294.0	0.842
$^{121}\text{Te}$	$(19.16 \pm 0.05)$ d	EC	507.6, 573.1	0.011
$^{113}\text{Sn}$	$(115.09 \pm 0.03)$ d	EC	27.9	0.8374
$^{109}\text{Cd}$	$(461.9 \pm 0.4)$ d	EC	25.5	0.8120
$^{22}\text{Na}$	$(2.6029 \pm 0.0008)$ y	EC, $\beta^+$	511	0.0050
			1274.6	0.0038
$^3\text{H}$	$(12.312 \pm 0.025)$ y	$\beta^-$		

#### 3.1. Iodine and tellurium isotopes

Initial activities underground were measured following the evolution of the identifying signatures for each isotope along several months; then, production rates at sea level were properly estimated according to the history of detectors. This ana-

## Study of the cosmogenic activation in NaI(Tl) crystals within the ANAIS experiment 7

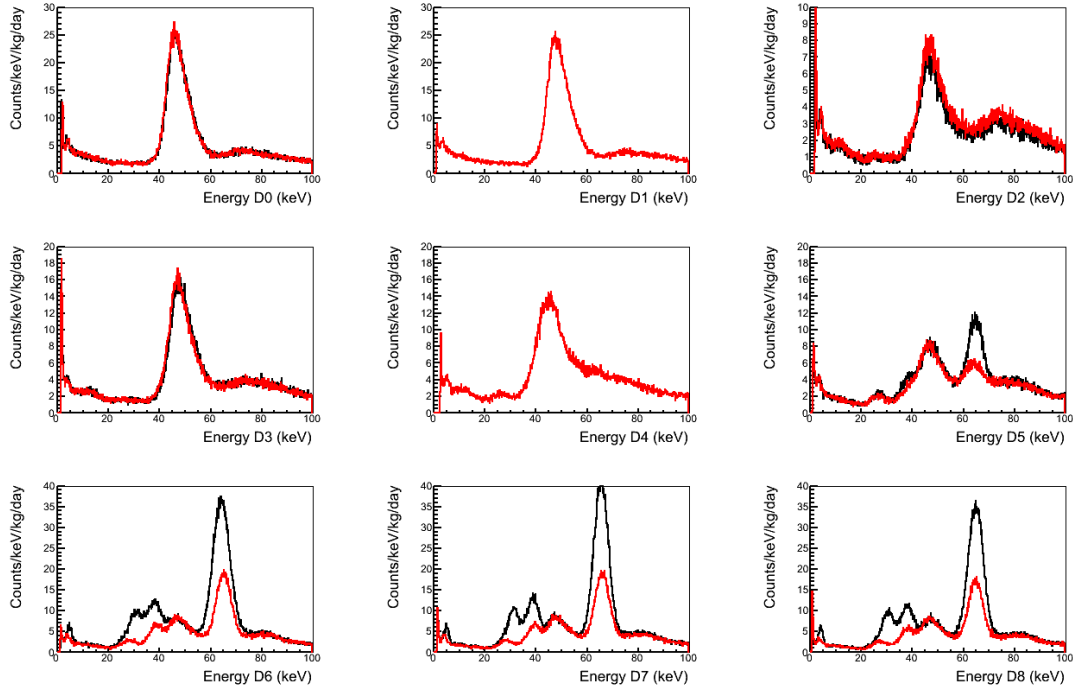


Fig. 2. Low energy region of the background spectra registered in the commissioning run of ANAIS-112. Data from the first 29.2 days (March and April, 2017) in black and the last 30.1 days (June and July, 2017) in red are shown (note they correspond to filtered spectra but with no cut efficiency correction yet). The short-lived isotopes have completely decayed in the detectors which arrived first to Canfranc (D0-D3) but their emissions are noticeable in the others (D4-D8). D1 and D4 dealt with some problems at the beginning of data taking (solved rapidly) and therefore data from the first 29.2 days in these detectors are not shown in this plot.

lysis was made only for D0 and D1 detectors in ANAIS-25 set-up for short-lived isotopes; but those results have been used for the rest of detectors when including the cosmogenics in the corresponding background models for the first data taken underground, reproducing successfully the measured spectra.

The distinctive signatures considered for the identification of each cosmogenically induced isotope listed in Table 2 have been analyzed, as well as the estimate of the corresponding detection efficiency  $\epsilon$  in ANAIS-25 set-up. For the metastable isotopes of Te, full energy depositions corresponding to the excited level energy have been considered. Activation has been assessed independently for each crystal, and whenever possible, results have been properly combined.

- For  $^{125}\text{I}$ , the peak at 67.3 keV was considered. Since this isotope decays with 100% probability by electron capture to an excited state of the Te daughter nucleus, this peak is produced by the sum of the energy of the excited level

(35.5 keV) and the binding energy of the K-shell of Te (31.8 keV). Efficiency for the detection of the energy deposition is expected to be  $\approx 100\%$ , hence the product  $I\epsilon$  is taken to be equal to the K-shell EC probability,  $I\epsilon = 0.8011$ .<sup>38</sup>

- For  $^{127m}\text{Te}$ , the peak at 88.3 keV, corresponding to the energy of the metastable state, has been analyzed. The branching ratio of the internal transition is  $I = 97.27\%$ <sup>38</sup> and 100% detection efficiency has been assumed. This signature for D1 detector could not be evaluated along data from March to June 2013 since a worse resolution hindered good fitting and therefore in this case final results come only from D0 detector.
- For  $^{125m}\text{Te}$ , the peak at 144.8 keV has been studied. Internal transition occurs with 100% probability and detection efficiency has been evaluated by simulation giving  $\epsilon = 0.968$ . In this case, it has been possible to quantify the peak, although not for all data sets and detectors; therefore, final results have been obtained only from D0 in the low energy spectrum.
- For  $^{123m}\text{Te}$ , the peak at 247.6 keV has been analyzed. The branching ratio of internal transition is 100%. The loss of efficiency due to the emission with 84% probability of a 159 keV photon<sup>38</sup> which can escape detection has been evaluated by Geant4 simulation giving an overall detection efficiency  $I\epsilon = 0.972$ .
- Similarly, for  $^{121m}\text{Te}$ , the peak at 294.0 keV has been analyzed and a correction factor to the detection efficiency has been estimated by means of Geant4 simulation to account for the probability of losing the 212 keV gamma ray which is emitted in 81% of the decays.<sup>40</sup> The branching ratio of internal transition is here 88.6%<sup>40</sup> and then the final value considered for  $I\epsilon$  is 0.842.
- A coincidence technique analysis has been applied to quantify  $^{126}\text{I}$  and  $^{121}\text{Te}$ , which decay by electron capture to excited states of the daughter nuclei. The identifying signature is the number of coincidences produced by the full absorption of high energy gamma emissions (see Table 2) in one detector and that corresponding to the binding energy for K-shell electrons in Te or Sb (31.8 or 30.5 keV, respectively) in the other detector. Just as an example, Fig. 3 shows the coincidence plot between detectors D0 and D1, obtained from the very beginning of data taking until February 2013 (210 days). By selecting a window from 15 to 45 keV in D1 data, we obtain the D0 coincident spectrum shown in Fig 3: peaks from  $^{121}\text{Te}$  and  $^{126}\text{I}$  are clearly observed and are used to determine the number of events attri-

butable to each isotope in a given time period. The product  $I\epsilon$  for these coincidence signals has been evaluated by simulating the decays of each isotope in the crystals with Geant4, obtaining  $I\epsilon = 0.0035$  for  $^{126}\text{I}$  and  $I\epsilon = 0.011$  for  $^{121}\text{Te}$ . These two isotopes have the shortest half-lives of all the analyzed products. The coincidence signal has been properly identified only within the first 42 days of available data for  $^{126}\text{I}$ . However, for  $^{121}\text{Te}$  the signal has not faded out since this isotope is being produced as result of the decay of the longer lived  $^{121m}\text{Te}$ , also cosmogenically induced; therefore, this point has been considered in the analysis of the time evolution of the coincidence signature of  $^{121}\text{Te}$ .

The evolution in time of the counting rates  $R$  for the different identifying signatures described above has been analyzed and is shown in the plots of Fig. 4 for I and metastable Te isotopes (the origin of absolute times has been chosen at 0 h on 28<sup>th</sup> November 2012, corresponding to the storage of detectors deep underground at LSC). Single exponential decays following the radioactive decay law are clearly observed in all of them. Fits of  $R$  vs. time have been carried out considering not only the combined signatures from each detector (shown for most of the products) but also the independent ones from D0 and D1. From the fit parameters, the half-lives  $T_{1/2}$  and initial activities underground  $A_0$  have been derived for each isotope, taking into account the described intensity  $I$  and efficiency  $\epsilon$  for the considered signals, and are summarized in Table 3. Error bars plotted in Fig. 4 represent for Y-axis the uncertainty of peak areas, which has been taken into account in the fits; for X-axis, they only indicate the time range signals have been evaluated over. As shown in Table 3, the half-lives deduced from the fits agree with the known values within uncertainties, confirming the choice of signatures for each isotope.

The initial activities  $A_0$  have been also deduced following a different approach, taking into consideration the decay of isotopes during the time intervals over which the identifying signatures are integrated. For an isotope with decay time constant  $\lambda$ , the expected number of events per unit mass of the detector  $C$  from time  $t_i$  to  $t_f$  is:

$$C = \frac{A_0 \cdot I\epsilon [\exp(-\lambda \cdot t_i) - \exp(-\lambda \cdot t_f)]}{\lambda} \quad (1)$$

An average of the  $A_0$  values deduced from Eq.(1) for each period of time has been obtained for each isotope, weighted with uncertainties coming from peak area estimates; results are shown in Table 3 too. The two methods give compatible results, although slightly lower values are systematically obtained from the second one.

Fig. 5 shows the evolution in time of the activity of  $^{121}\text{Te}$  deduced from its

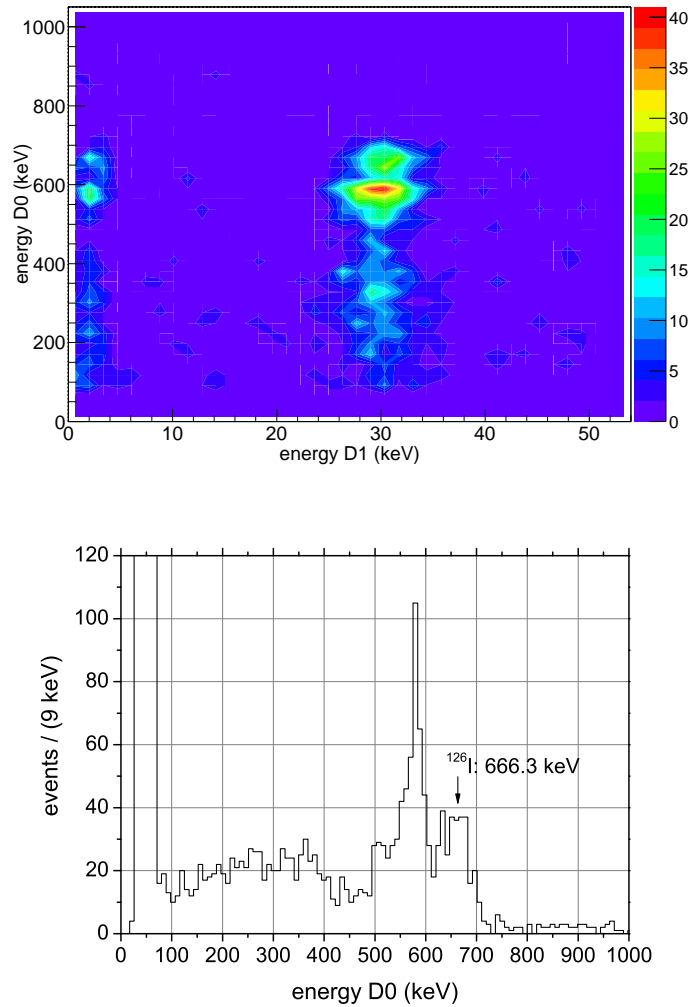


Fig. 3. (Top): Coincidence plot between D0 and D1 in the beginning of data taking. Coincidences due to both  $^{126}\text{I}$  and  $^{121}\text{Te}$  between high energy photons absorbed in D0 and the binding energies of Te or Sb registered in D1 are clearly seen, for K shell (around 31 keV) and even for L-shell (around 5 keV). D0 energies below 80 keV have been cut because the high rate of coincidences there prevents from seeing  $^{126}\text{I}$  and  $^{121}\text{Te}$  coincidences. (Bottom): Spectrum of the high energy D0 data in coincidence with a window in D1 data around K shell binding energies of Te and Sb; peaks at 507.6-573.1 and 666.3 keV are singled out and then, activities of these isotopes can be quantified.

identifying signature adding D0 and D1 data. A single exponential decay with the half-life of  $^{121}\text{Te}$  is not observed in this case because the isotope is being produced by the decay of  $^{121m}\text{Te}$ , also cosmogenically induced and having a longer half-life.

A different fitting function is needed to derive the initial activity underground and to estimate the production rate at sea level for  $^{121}\text{Te}$ .

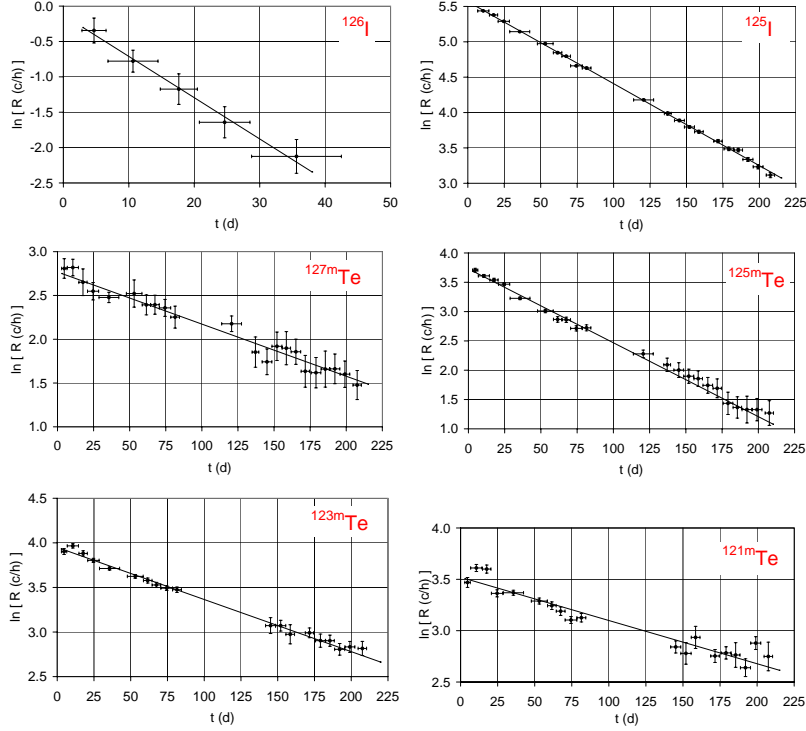


Fig. 4. Evolution in time of the logarithm of the counting rate  $R$  (expressed in counts per hour) assigned to each isotope, calculated as the addition of the rates in D0 and D1 detectors. Only for  $^{127m}\text{Te}$  and  $^{125m}\text{Te}$  results correspond to rate measured with D0 detector. The corresponding fits are also shown (solid line). Error bars on X-axis only indicate the time range signals have been evaluated over.

The time dependence of the activity of  $^{121}\text{Te}$  during the data taking in ANAIS-25 can be written as the addition of two terms, corresponding to the decay of the cosmogenically produced  $^{121}\text{Te}$  and to the production, and subsequent decay, of  $^{121}\text{Te}$  from  $^{121m}\text{Te}$ :

$$A(t) = \lambda_g N_{0,g} \exp(-\lambda_g t) + P_{IT} N_{0,m} \frac{\lambda_g \lambda_m}{\lambda_g - \lambda_m} [\exp(-\lambda_m t) - \exp(-\lambda_g t)] \quad (2)$$

with subindex  $g(m)$  referring to the ground (metastable) states of the isotope and being  $N_0$  the initial number of nuclei and  $P_{IT} = 0.886$  the probability of internal transition of the metastable state. To obtain the initial number of nuclei, and then, the corresponding activities, for both the ground and metastable states, several fits

Table 3. Results derived for each cosmogenic product from the selected detectors and data periods: half-lives  $T_{1/2}$  and initial activities underground  $A_0$  from the fits of R vs time and average  $A_0$  from activities obtained from time intervals considering the isotope decay (see text). The known values of the half-lives, presented in Table 2, are included again for comparison. Results for  $^{126}\text{I}$  correspond to data from the start of data taking until February 2013 and results for  $^{125}\text{I}$ ,  $^{127m}\text{Te}$ ,  $^{125m}\text{Te}$ ,  $^{123m}\text{Te}$  and  $^{121m}\text{Te}$  correspond to data from the start of data taking until June 2013.

Isotope	$T_{1/2}$ (days)	Detector	Fitted $T_{1/2}$ (days)	Fitted $A_0$ ( $\text{kg}^{-1}\text{d}^{-1}$ )	Average $A_0$ ( $\text{kg}^{-1}\text{d}^{-1}$ )
$^{126}\text{I}$	$12.93 \pm 0.05$	D0 + D1	$11.9 \pm 1.7$	$483 \pm 77$	$430 \pm 37$
$^{125}\text{I}$	$59.407 \pm 0.009$	D0 + D1	$59.80 \pm 0.26$	$627.6 \pm 2.4$	$621.8 \pm 1.6$
$^{127m}\text{Te}$	$106.1 \pm 0.7$	D0	$116.4 \pm 8.1$	$31.5 \pm 1.3$	$32.1 \pm 0.8$
$^{125m}\text{Te}$	$57.40 \pm 0.15$	D0	$55.0 \pm 1.1$	$82.6 \pm 1.2$	$79.1 \pm 0.8$
$^{123m}\text{Te}$	$119.3 \pm 0.1$	D0 + D1	$118.6 \pm 3.1$	$102.5 \pm 1.2$	$100.8 \pm 0.8$
$^{121m}\text{Te}$	$164.2 \pm 0.8$	D0 + D1	$164.6 \pm 9.3$	$77.1 \pm 1.7$	$76.9 \pm 0.8$

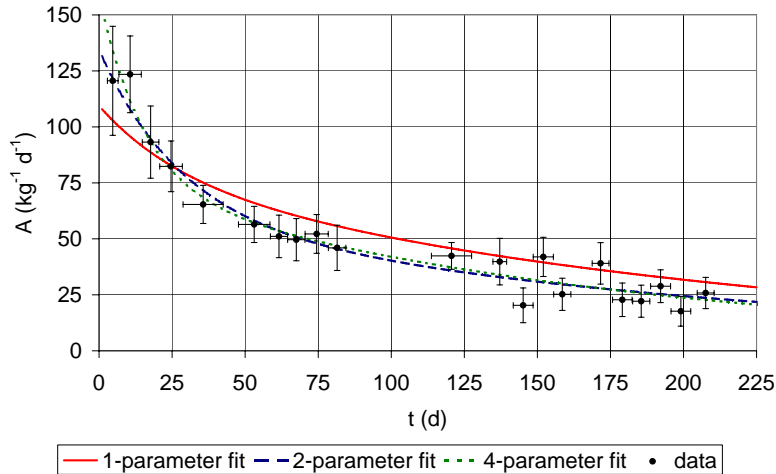


Fig. 5. Evolution in time of the  $^{121}\text{Te}$  activity deduced from the identifying signature summed from D0 and D1; the lines show the corresponding fits to Eq.(2), considering 1 (red solid line), 2 (blue dashed line) and 4 (green dotted line) free parameters (see text).

to the dependence given by Eq.(2) for the signal from  $^{121}\text{Te}$  have been tried and are also plotted in Fig. 5. One fit has been performed letting four parameters free: the activities  $A_{0,g} = N_{0,g} \lambda_g$  and  $A_{0,m} = N_{0,m} \lambda_m$  and the half-lives  $T_{1/2,g}$  and  $T_{1/2,m}$ . Other fit has been made with two free parameters, fixing the two half-lives according to the known values reported in Table 2. The last fit has been carried out with only one free parameter, fixing in addition the activity of the metastable state to the average of the two estimates given in Table 3:  $A_{0,m} = 77.0 \text{ kg}^{-1}\text{d}^{-1}$ . The product  $I_e$  presented in Table 2 has been used. All the fit results are presented in Table 4. The three estimates of the initial activity underground for  $^{121}\text{Te}$  are reasonably compatible within uncertainties and those for  $^{121m}\text{Te}$  are of the same

order than the value deduced before (see Table 3). The half-lives deduced in the first fit reported in Table 4 are in the  $2\sigma$  interval of the known values. The  $^{121}\text{Te}$  activity obtained from the 1-parameter fit will be used to estimate the production rate as it takes into account all known information and then, minimizes the contribution from systematics.

Table 4. Initial activities underground and half-lives derived for the metastable and ground states of  $^{121}\text{Te}$  by fitting the signal plotted in Fig. 5 to the dependence given by Eq.(2) with different sets of free parameters (see text).

Fit	$A_{0,m}$ ( $\text{kg}^{-1}\text{d}^{-1}$ )	$A_{0,g}$ ( $\text{kg}^{-1}\text{d}^{-1}$ )	$T_{1/2,m}$ (d)	$T_{1/2,g}$ (d)
4 parameters	$76 \pm 15$	$159 \pm 33$	$122 \pm 27$	$10.5 \pm 5.4$
2 parameters	$59.3 \pm 3.9$	$134 \pm 13$	-	-
1 parameter	-	$110 \pm 12$	-	-

As it has been indicated before, ANAIS crystals were built in Alpha Spectra facilities in Grand Junction, Colorado. The history of the starting material used to produce the NaI powder from which crystals are grown is unknown; this exposure along geological time scales must be relevant only for very long-lived isotopes like  $^{129}\text{I}$  or  $^{123}\text{Te}$ , for those having shorter lifetimes saturation would have been probably reached independently from previous exposure history while purifying, growing the crystals and building the detectors (except maybe for  $^{22}\text{Na}$ ). Colorado is placed at a quite high altitude; consequently, a very important correction factor  $f$  to the cosmic neutron flux at New York City coordinates is reported at Ref. 41 for Colorado locations due to altitude and geomagnetic rigidity (4.11 and even 12.86 for Denver and Leadville, respectively). Afterwards, detectors were transported to LSC by boat and by road, being the travel duration about one month, most of the time at sea level. Therefore, the initial activities underground derived here cannot be directly considered the saturation activities (i.e. production rates,  $R_p$ ) at sea level. However, in the following a method to estimate the production rates in our crystals, based on a few reasonable assumptions, is proposed. Considering that saturation activity is reached at a given place characterized by a correction factor  $f$  to the cosmic neutron flux at sea level, the number of nuclei cosmogenically induced for a particular isotope is  $N_{sat} = fR_p/\lambda$ . If the material is then exposed to cosmic rays at sea level for a time  $t$ , it is straightforward to derive the posterior evolution of the corresponding activity by solving the usual differential equation with simultaneous production and decay of a nuclear species for an initial number of nuclei  $N_{sat}$ :

$$A(t) = R_p[1 + (f - 1)\exp(-\lambda t)] \quad (3)$$

The production rate  $R_p$  of an isotope can be obtained from Eq.(3) using its

initial activity underground, and fixing the correction factor  $f$  and exposure time at sea level  $t$ . Table 5 summarizes the production rates obtained in this way for  $f = 3.6 \pm 0.1$ ,  $t = 30 \pm 5$  days,  $\lambda$  from  $T_{1/2}$  values in Table 2 and the average  $A_0$  values presented in Table 3 (considering the isotope decay along the data taking) and Table 4. The correction factor  $f$  was estimated specifically for Grand Junction altitude.<sup>33</sup> The estimate of the production rate of  $^{121}\text{Te}$  from the measured initial activity underground is not so easy due to the combination of direct production and production through the metastable state; the procedure applied was described in detail in Ref. 33.

Table 5. Production rates at sea level  $R_p$  deduced for all the identified cosmogenic isotopes in ANAIS detectors (in  $\text{kg}^{-1}\text{d}^{-1}$ ) (see text).

Isotope	$^{126}\text{I}$	$^{125}\text{I}$	$^{127m}\text{Te}$	$^{125m}\text{Te}$	$^{123m}\text{Te}$	$^{121m}\text{Te}$	$^{121}\text{Te}$	$^{113}\text{Sn}$	$^{109}\text{Cd}$	$^{22}\text{Na}$
$R_p$ ( $\text{kg}^{-1}\text{d}^{-1}$ )	$283 \pm 36$	$220 \pm 10$	$10.2 \pm 0.4$	$28.2 \pm 1.3$	$31.6 \pm 1.1$	$23.5 \pm 0.8$	$9.9 \pm 3.7$	$6.8 \pm 1.6$	$2.0 \pm 0.6$	$45.1 \pm 1.9$

There are other isotopes, also cosmogenically produced, that have not been identified in this analysis, although they are probably present in ANAIS crystals. It is worth to mention the cases of  $^{129}\text{I}$  and  $^{123}\text{Te}$ .

$^{129}\text{I}$  can be produced by uranium spontaneous fission and by cosmic rays. Its concentration is strongly affected by the ore material exposure either to cosmic rays or to high uranium content environment. It presents 100%  $\beta^-$  decay to the excited level of 39.6 keV of the daughter nucleus with a half-life  $T_{1/2} = (16.1 \pm 0.7) \cdot 10^6$  y,<sup>38</sup> being hence the expected signature in large NaI(Tl) crystals a continuous beta spectrum starting in 39.6 keV. This signal is above the region of interest (RoI) for dark matter searches, but it is important for a complete understanding of the background.<sup>36</sup> The long lifetime and the difficulty to disentangle the signature from other emissions are the reasons why the quantification of the amount of  $^{129}\text{I}$  in ANAIS crystals was not possible. In Ref. 42 the estimated fraction of this isotope was determined to be  $^{129}\text{I}/^{nat}\text{I} = (1.7 \pm 0.1) \cdot 10^{-13}$ ; however, strong variability of this concentration is expected in different origin ores.

In the case of  $^{123}\text{Te}$ , we expect the presence of this isotope as daughter of the metastable state  $^{123m}\text{Te}$ , effectively identified, and probably also directly produced by cosmic rays by similar reaction mechanisms. This isotope would decay 100% following EC to the ground state of the daughter nucleus, having a half-life larger than  $10^{13}$  y.<sup>40</sup> The signature in ANAIS detectors would be a peak corresponding to the full absorption of the binding energy of L-shells of Sb. For the moment, this signal cannot be resolved from other contributions from Te/I isotopes still present, having L-shell EC in higher or lower extent.

### 3.2. $^{22}\text{Na}$

$^{22}\text{Na}$  is specially worrisome for dark matter searches because the binding energy of the K-shell of its daughter Ne is 0.87 keV, falling the corresponding energy deposition in the RoI, and having a long enough half-life to compromise the first years of data taking. The initial activity in crystals when moving underground has been estimated for the nine modules used in ANAIS-112, being different as the exposure history was not the same for all the detectors. Indeed, a shelter for cosmic rays was used during production for some of the detectors. In addition, an estimate of the production rate was derived from the results of ANAIS-25.

In detectors D0 and D1, cosmogenically activated  $^{22}\text{Na}$  was identified and quantified using coincidence spectra in data from March 2014 to June 2014. The analyzed signature was the integral number of events from 2300 to 2900 keV (corresponding to full absorption of its positron and gamma emissions) in the spectrum obtained summing D0 and D1 energies, for coincidence events leaving 511 (or 1275) keV at any detector. These were the best signatures found for this isotope to avoid the interference of backgrounds. The product  $I\epsilon$  for these signals was evaluated by Geant4 simulation of  $^{22}\text{Na}$  decays in the crystals, obtaining  $I\epsilon = 0.0050$  for the 511 keV peak and  $I\epsilon = 0.0038$  for the 1275 keV signal. Fig. 6 (top) shows the coincidence spectra of D0 and D1 modules for data from March 2014 to June 2014. Fig. 6 (bottom) presents the total energy spectra (summing D0 and D1 energy) obtained for events selected by a 511 keV (1275 keV) energy deposition in one detector, fixing a window at  $\pm 1.4\sigma$ . Only the region between 2300 and 2900 keV was used for the rate estimate. The effect of coincidences not due to  $^{22}\text{Na}$  has been taken into account subtracting their contribution in the 2300-2900 keV region, evaluated from events in a window on the left of the 511 keV peak and on the right of the 1275 keV peak. The presence of  $^{22}\text{Na}$  events on the subtracted background from shifted windows has not been considered, although it seems to be not very relevant (around 0.7% of the events selected for the considered signature could have been misidentified as background and subtracted).

Table 6. Measured activity  $A$  of  $^{22}\text{Na}$  from March to June 2014 and the deduced initial activity underground  $A_0$  considering the identifying signal for coincident events leaving 511 or 1275 keV at one detector (see text). These activities independently estimated have been properly averaged to derive the final result.

Signature (keV)	$A$ ( $\text{kg}^{-1} \text{d}^{-1}$ )	$A_0$ ( $\text{kg}^{-1} \text{d}^{-1}$ )
511	$109.0 \pm 4.3$	$158.2 \pm 6.3$
1275	$111.8 \pm 5.5$	$162.2 \pm 8.0$
mean	$110.0 \pm 3.4$	$159.7 \pm 4.9$

From the net number of events registered in the 2300-2900 keV region and the estimated  $I_e$  value reported at Table 2 the activity  $A$  of  $^{22}\text{Na}$  at measuring time has been evaluated and then the initial activity underground  $A_0$  deduced, using its half-life from Table 2. Table 6 presents the results, for both 511 and 1275 keV windows. In Fig. 6 (bottom) the measured spectra of the summed energy of D0 and D1 are compared with the corresponding simulations normalized with the deduced  $^{22}\text{Na}$  activity; the spectra shapes follow reasonably the expectation, somehow validating the method applied to single out  $^{22}\text{Na}$  contribution. From the mean value of  $A_0$  in Table 6 the production rate of  $^{22}\text{Na}$  at sea level was also estimated, as shown in Table 5.

Table 7. Comparison of cosmogenically produced  $^{22}\text{Na}$  initial activity,  $A_0$ , estimates (in  $\text{kg}^{-1} \text{d}^{-1}$ ) for ANAIS detectors in different set-ups (see text).

Detector	ANAIS-25 <sup>33</sup>	ANAIS-37 <sup>35</sup>	A37D3	ANAIS-112
D0	$159.7 \pm 4.9$	$158.4 \pm 7.9$	$164 \pm 17$	$155 \pm 11$
D1	$159.7 \pm 4.9$			$168 \pm 11$
D2		$70.2 \pm 3.9$	$57.6 \pm 8.1$	$43.9 \pm 6.0$
D3			$69.9 \pm 3.6$	$68.6 \pm 4.6$
D4				$61.8 \pm 3.1$
D5				$43.7 \pm 2.3$
D6				$53.8 \pm 2.7$
D7				$55.6 \pm 2.7$
D8				$56.4 \pm 2.8$

A direct estimate of  $^{22}\text{Na}$  activity in D2 crystal was carried out by analyzing coincidences from data corresponding to 111.4 days (live time) from a special set-up taking data from October 2015 to February 2016 where only D0 and D2 detectors were used; in particular, profiting from the reduced cosmogenic contribution to the background in this period after enough cooling time underground, D2 spectrum in coincidence with 1275 keV depositions in D0 was analyzed. The obtained value for the initial activity (corresponding to the moment of storing crystals deep underground at LSC),  $A_0 = (70.2 \pm 3.9) \text{kg}^{-1} \text{d}^{-1}$ , was more than a factor of two lower than the one deduced for D0 and D1 detectors.<sup>35</sup> This result was compatible with a lower time of exposure of D2 to cosmic rays, taking into account the  $^{22}\text{Na}$  half-life, longer than that corresponding to I and Te products. It is worth noting that the  $^{22}\text{Na}$  initial activity in D0 deduced from the analogue analysis is in perfect agreement with the first estimate in ANAIS-25 set-up (see Table 7).

A procedure to quantify the initial activities of  $^{22}\text{Na}$  in the rest of detectors analogue to that followed for D2 has been applied in different set-ups with three crystals and in ANAIS-112 with nine crystals, looking for coincidences with 1275 keV de-

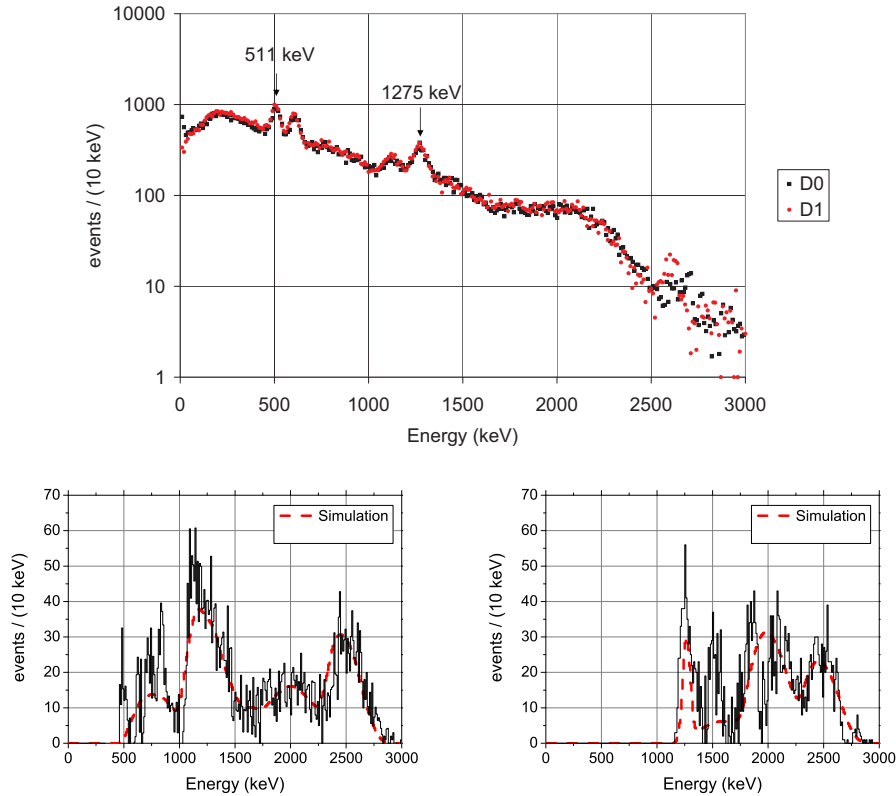


Fig. 6. Top: Energy spectra of D0 (black squares) and D1 (red circles) registered for coincidences between them for data from March 2014 to June 2014. Bottom: Spectrum of the summed energy of D0 and D1 for events in a  $\pm 1.4\sigma$  window around the 511 (left) and 1275 keV (right) peaks in any of the coincidence spectra. Background coincidences have been estimated (see text) and subtracted.  $^{22}\text{Na}$  signature has been evaluated from the region between 2300 and 2900 keV (corresponding to full absorption of its positron and gamma emissions). Measured spectra are compared with simulations normalized with the deduced  $^{22}\text{Na}$  activity.

positions in other detectors. In particular, data from August to November 2017 collected in ANAIS-112 have been considered. Preliminary results from ANAIS-112 together with all the available previous estimates are summarized in Table 7. The initial activity for D0 and D1 was significantly larger than for the other detectors produced afterwards, pointing at a reduction on the exposure time while crystal growing and detector building at Colorado. Whenever estimates from different setups are available, a reasonable agreement between them is obtained.

### 3.3. $^3\text{H}$

Tritium is a relevant background in the RoI for the dark matter signal. In the ANAIS detectors, after a detailed analysis of several cosmogenic products,<sup>33</sup> the presence of tritium is inferred in order to explain the differences between the measured background and the background models.<sup>35</sup>

It is a pure beta emitter with transition energy of 18.591 keV and a long half-life of 12.312 y.<sup>38</sup> Following the shape of the beta spectrum for the super-allowed transition of  $^3\text{H}$ , 57% of the emitted electrons are in the range from 1 to 7 keV; these electrons are typically fully absorbed since most of the dark matter detectors are large enough. Due to the long half-life of tritium, saturation activity is difficult to reach; however, even below saturation, as tritium emissions are concentrated in the energy region where the dark matter signal is expected, tritium can be important. Quantification of tritium cosmogenic production is not easy, neither experimentally since its beta emissions are hard to disentangle from other background contributions, nor by calculations, as tritium can be produced by different reaction channels. Tritium production in materials of interest for dark matter experiments has been studied in Ref. 43.

Although a direct identification of a tritium content in the crystals has not been possible, the construction of a detailed background model of the firstly produced detectors (based on a Geant4 simulation of quantified background components) points to the need of an additional background source contributing only in the very low energy region, which could be tritium.<sup>35,44</sup> The simulated spectra including all well-known contributions agree reasonably with the ones measured, except for the very low energy region; as shown in Fig. 7, the inclusion of a certain activity of  $^3\text{H}$  homogeneously distributed in the NaI crystal provides a very good agreement also below 20 keV. Fig. 7 compares data and background models for D0 and D2. The shown data correspond to 59.9 days of measurement in September and October 2016. No fitting has been attempted, but the required  $^3\text{H}$  initial activities to reproduce the data would be around 0.20 mBq/kg for D0 and 0.09 mBq/kg for D2, that is, different for the two detectors. The latter value is just the upper limit set for DAMA/LIBRA crystals.<sup>42</sup>

Preliminary background models developed for the other ANAIS detectors already operated in Canfranc point to a tritium content similar to that assumed for D2 (see Fig. 7 for D8). Since the exposure history of the NaI material used to produce the crystals (following different procedures for purification and crystal growth) is not precisely known, no attempt of deriving tritium production rates from these estimated activities in ANAIS crystals has been made. But some cross-check of the results is possible to confirm the plausibility of the tritium hypothesis; assuming that the whole crystal activation took place in Alpha Spectra facilities at Grand

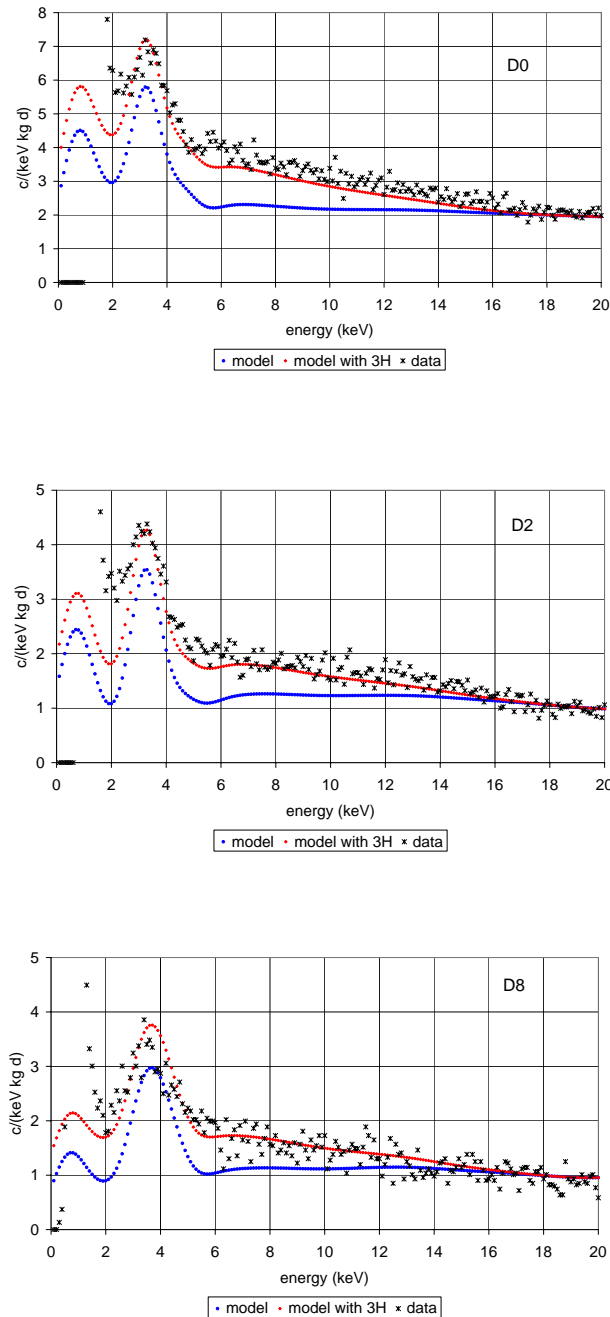


Fig. 7. The very low energy region of the energy spectra measured for D0 (top), D2 (center) and D8 (bottom) ANAIS detectors compared with the corresponding simulated models<sup>35</sup> including all the quantified intrinsic and cosmogenic activities in the detectors and main components of the set-up (blue) and adding also tritium in the NaI crystal (red). D0 and D2 data correspond to September - October 2016 in A37D3 and D8 data corresponds to commissioning run of ANAIS-112 from June - July 2017. A  $^3\text{H}$  activity of 0.20 mBq/kg is considered for D0 and 0.09 mBq/kg for D2 and D8.

Junction, Colorado (where the cosmic neutron flux is estimated to be a factor  $f = 3.6$  times higher than at sea level<sup>33</sup>) the required exposure time  $t_{exp}$  to produce an activity  $A$  of an isotope with decay constant  $\lambda$  for a production rate  $R$  at sea level can be deduced using

$$A = f \cdot R[1 - \exp(-\lambda \cdot t_{exp})] \quad (4)$$

For the range of estimated production rates in Ref. 43 (see section 4) and the deduced tritium activities in D0 and D2, the exposure times are between 0.8 and 1.6 years and 4.2 and 8.4 months, respectively. These values roughly agree with the time lapse between sodium iodide raw material purification starting and detector shipment, according to the company. As an additional check, for these exposure times, the ratio of the induced initial activities of the also long-living cosmogenic isotope  $^{22}\text{Na}$  in D0 and D2 following Eq.(4) is  $\sim 2$ , in good agreement with the measured activities<sup>33,35</sup> (see Table 7). Since purification methods cannot remove this isotope, this means that the raw material was not significantly exposed to cosmic rays before.

### 3.4. $^{113}\text{Sn}$ and $^{109}\text{Cd}$

In the first analysis of cosmogenic activation carried out using ANAIS-25 data,<sup>33</sup> the presence of  $^{113}\text{Sn}$  and  $^{109}\text{Cd}$  in the NaI(Tl) crystals was not observed; however, the study of the background measured in D0, D1 and D2 detectors performed in the long term allowed to identify signals from these two isotopes.<sup>35</sup>

As summarized in Table 2,  $^{113}\text{Sn}$  decays by electron capture mainly to a 391.7 keV isomeric state of the daughter, having a half-life of 115.1 days; therefore, a peak at the binding energy of K-shell electrons of In at 27.9 keV is produced, as well as another one for the L-shell at around 4 keV. The ratio between the probabilities of electron capture for K and L shells is 7.4 for decay to the isomeric state.<sup>38</sup> Similarly,  $^{109}\text{Cd}$  decays by electron capture to the 88-keV isomeric state of the daughter, having a half-life of 461.9 days, and therefore it gives a peak at the binding energy of the K-shell of Ag at 25.5 keV together with an additional peak around 3.5 keV, corresponding to the Ag L-shell binding energy (being 5.4 the ratio between K and L-shell EC probabilities<sup>38</sup>).

For the ANAIS detectors operated in the different set-ups, the following behavior has been observed: once the tellurium and iodine cosmogenic isotopes decaying by EC have significantly decayed, the large peak produced at the K-shell binding energies of Sb and Te (see plots for D6-D8 in Fig. 2) disappears and a line at  $\sim 28$  keV can be identified, which also fades away within a few months; then, the contribution at 25 keV is visible, decreasing in time more slowly. Although a precise

time analysis cannot be attempted as the peaks are very small, even if accumulated over long times, and cannot be resolved, the observed behavior seems compatible with the hypothesis that those peaks can be attributed to the decays of  $^{113}\text{Sn}$  and  $^{109}\text{Cd}$  cosmogenically produced in the NaI(Tl) crystals.

A quantification of the induced activities and the corresponding production rates of these two isotopes is underway profiting from data taken in the ANAIS crystals along different times; preliminary results from ANAIS-112 in 2017 are presented here. The  $I\epsilon$  values for the signals registered at the K-shell binding energies are reported in Table 2. The signals have been analyzed in spectra accumulated over a quite long time to make them measurable (see Fig. 8); the whole area of the peaks is assumed to be due just to one of the isotopes in the analyzed runs; then, from Eq.(1), the induced activity is deduced and, as explained in section 3.1 for tellurium and iodine isotopes, the production rate can be estimated from Eq.(2). Table 8 presents the initial activities obtained for several detectors and the deduced production rates, which being compatible within uncertainties, and because the exposure history of the detectors is supposed to be very similar, have been averaged (see Table 5). The live times for the runs considered are 30.1 days for June-July, 26.7 days for August and 25.8 days for November-December. The days after moving the detectors underground at the beginning (June 2017) and at the end (December 2017) of the data used in this analysis are 206 and 393 days for detectors D4-D5 and 85 and 272 days for detectors D6-D8. It is worth noting that, as it can be seen in Fig. 2, the signatures analyzed here to identify  $^{113}\text{Sn}$  and  $^{109}\text{Cd}$  are imperceptible in detectors D0-D3, which have been underground for more than 500 days at the time presently considered.

Table 8. Preliminary results for the initial activities  $A_0$  and production rates at sea level  $R_p$  for  $^{113}\text{Sn}$  and  $^{109}\text{Cd}$  deduced from data of several detectors taken in ANAIS-112 along the year 2017.

Isotope	Detector	Data	$A_0$ ( $\text{kg}^{-1}\text{d}^{-1}$ )	$R_p$ ( $\text{kg}^{-1}\text{d}^{-1}$ )
$^{113}\text{Sn}$	D6	June-July	$18.4\pm 9.5$	$5.8\pm 3.0$
	D7	June-July	$26.7\pm 8.9$	$8.4\pm 2.8$
	D8	June-July	$19.7\pm 7.9$	$6.2\pm 2.5$
	average			$6.8\pm 1.6$
$^{109}\text{Cd}$	D4	June-July	$5.3\pm 3.1$	$1.5\pm 0.9$
	D5	June-July	$8.8\pm 4.2$	$2.5\pm 1.2$
	D5	August	$9.4\pm 6.5$	$2.7\pm 1.9$
	D5	November-December	$9.6\pm 7.7$	$2.7\pm 2.2$
	average			$2.0\pm 0.6$

Peaks around 3.5 and 4 keV are expected too from  $^{109}\text{Cd}$  and  $^{113}\text{Sn}$  decays, corresponding to the binding energies of the L-shells of Ag and In, respectively, just in the RoI for dark matter searches. Therefore, these isotopes must be taken into

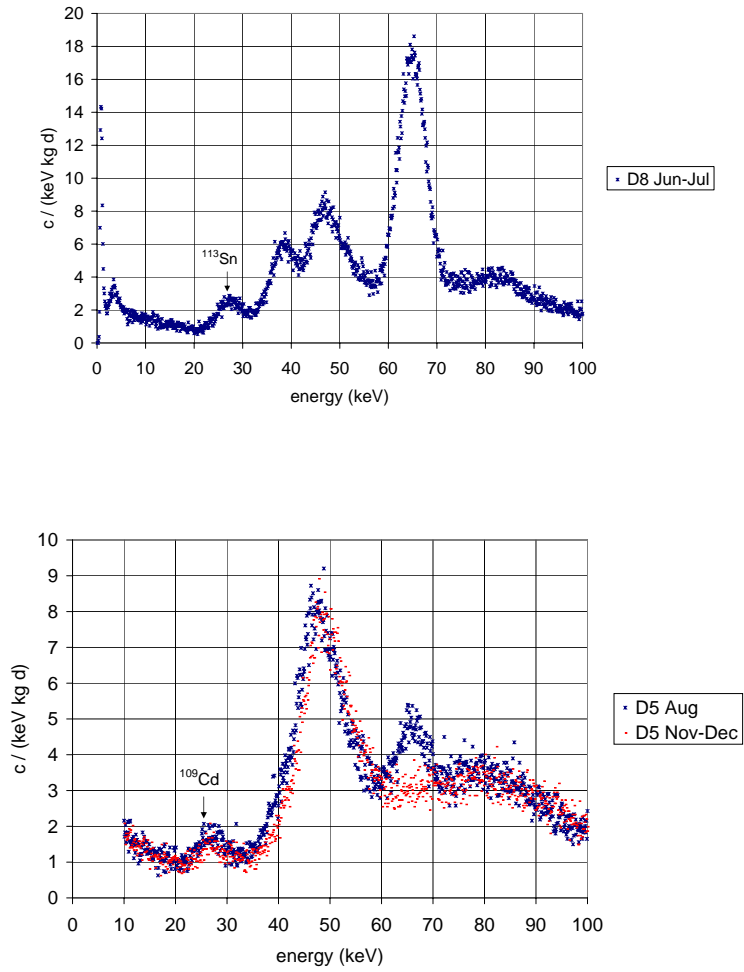


Fig. 8. Examples of the energy spectra considered in the quantification of  $^{113}\text{Sn}$  (top) and  $^{109}\text{Cd}$  (bottom) signals from the ANAIS-112 data: spectrum of D8 detector taken during June-July 2017 used for  $^{113}\text{Sn}$  (top) and those of D5 detector during August and November-December in 2017 used for  $^{109}\text{Cd}$  (bottom). Very similar spectra are registered for equivalent detectors and runs. Note that the dark matter run of ANAIS-112 started on 3<sup>rd</sup> August 2017 and data of the very low energy region are blinded since then.

account in the background models of NaI(Tl) detectors; as the half-lives, especially for  $^{113}\text{Sn}$ , are not too large, they should not be a problem in the long term.

#### 4. Calculation of production rates

As pointed out before, cosmogenic activation of materials is an hazard for experiments looking for rare events and therefore it must be properly assessed in the background models of this type of experiments. Production rates are the main input to compute the induced activities of the relevant isotopes. Since direct estimates of the production rates, as those presented here for NaI, are not available for all materials and products, in many cases production rates must be evaluated using Eq.(5) from the cosmic ray flux  $\phi$  and the production cross sections  $\sigma$ , both dependent on the energy  $E$  of cosmic particles:

$$R_p \propto \int \sigma(E)\phi(E)dE \quad (5)$$

This calculation method is strongly dependent on the excitation functions and assumed cosmic ray spectrum. In order to validate different approaches to such a calculation, production rates at sea level for all the cosmogenic products identified and quantified in ANAIS crystals will be evaluated and then compared with the values obtained from the measurements presented in section 3. Although not observed in ANAIS-25 data mainly due to its short half-life ( $T_{1/2} = (4.1760 \pm 0.0003)$  days),  $^{124}\text{I}$  has been considered in this study too. Production rate of  $^{123}\text{Te}$ , having low energy emissions dangerous for dark matter searches, has been also evaluated.

One of the most relevant processes in cosmogenic activation is the spallation of nuclei by high energy nucleons, but other reactions like fragmentation, induced fission or capture can be also very important for some nuclei. It must be taken into account that at sea level, nuclide production is mainly dominated by neutrons at low energies, whereas if materials are flown at high altitude cosmic flux is much greater, energies at play are larger and therefore activation by protons can not be neglected.

The excitation function for the production of a certain isotope by nucleons in a target over a wide range of energies (from some MeV up to several GeV) can be hardly obtained only from experimental data, since the measurements of production cross-sections with beams are demanding. The use of computational codes is therefore mandatory, although experimental data are essential to check the reliability of calculations. The difficulties for properly describing excitation functions are discussed for instance at Ref. 45.

Most of the considered cosmogenic isotopes are induced by interactions on  $^{127}\text{I}$ ; only  $^{22}\text{Na}$  is produced on  $^{23}\text{Na}$ . Both  $^{127}\text{I}$  and  $^{23}\text{Na}$  have a 100% isotopic abundance in natural iodine and sodium, respectively.

Table 9 presents the obtained production rates for the analyzed cosmogenic iso-

topes considering the selected excitation functions; a discussion on the suitability of the considered codes and libraries for obtaining cross sections in this study can be found in Ref. 33. For the cosmic ray spectrum, the parametrization from Gordon et al.<sup>46</sup> (valid for energies above 0.4 MeV and obtained from a set of measurements of cosmic neutrons on the ground across the US using Bonner sphere spectrometers) has been considered. Results are given per day and per kg of NaI. Contributions from the low energy (LE) and high energy (HE) descriptions of the cross sections are shown together with the total rate. For most of the isotopes, the dominant contribution comes from the low energy region; for instance, for iodine isotopes it accounts for  $\approx 90\%$  of the rate.

Table 9 shows also the production rates deduced experimentally for comparison. Ratios between the calculated and experimental rates are given too. Good agreement has been found for I isotopes, having cross sections well validated not only at high energy with protons but also at low energies with neutrons. Given the discrepancies found between calculated and experimental production rates, it can be concluded that calculations of activation yields in sodium iodide for ultra-low background experiments are reasonable and the used cross sections are well validated along all the relevant energy range.

Table 9. Production rates (in  $\text{kg}^{-1}\text{d}^{-1}$ ) calculated from Eq.(5) using different selections of the excitation function (indicated in the second column) showing the contributions from LE and HE ranges and the total rate. Production rates obtained experimentally in Table 5 are shown for comparison. Last column presents the ratio between the calculated and the experimental rates.

Isotope	Excitation function LE+HE	Calculation rate LE+HE	Total	Experimental rate	Cal/Exp
<sup>126</sup> I	MENDL-2 + YIELDX	250.0+ 47.0	292.0	283 ± 36	1.1
<sup>125</sup> I	TENDL-2013 + HEAD2009	230.2 + 12.1	242.3	220 ± 10	1.1
<sup>124</sup> I	MENDL-2 + HEAD2009	113.6 + 22.3	135.9		
<sup>127m</sup> Te	TENDL-2013 + extrapolation	6.9 + 0.2	7.1	10.2 ± 0.4	0.7
<sup>125m</sup> Te	TENDL-2013 + HEAD2009	38.4 + 3.5	41.9	28.2 ± 1.3	1.5
<sup>123m</sup> Te	TENDL-2013 + HEAD2009	29.5 + 3.7	33.2	31.6 ± 1.1	1.1
<sup>123</sup> Te	TENDL-2013 + HEAD2009	8.8 + 1.4	10.2		
<sup>121m</sup> Te	TENDL-2013 + HEAD2009	19.1 + 4.7	23.8	23.5 ± 0.8	1.0
<sup>121</sup> Te	TENDL-2013 + YIELDX	5.8 + 2.6	8.4	9.9 ± 3.7	0.8
<sup>113</sup> Sn	TENDL-2014 + HEAD2009	3.3 + 6.6	9.9	6.8 ± 1.6	1.5
<sup>109</sup> Cd	TENDL-2014 + HEAD2009	0.5 + 1.1	1.6	2.0 ± 0.6	0.8
<sup>22</sup> Na	TENDL-2013 + YIELDX	43.2 + 1.4	53.6	45.1 ± 1.9	1.2

The calculation of the production rate of tritium is of particular interest as there is no experimental estimate and it has been addressed in Ref. 43 following a similar procedure to that applied to other isotopes. Fig. 9 shows the compilation of production cross sections for iodine and sodium taken from different sources. It is

not evident which is the best description of the excitation functions for the tritium production considered here. For the lowest energies, the TENDL data for neutrons up to 200 MeV reproduce well the measurement on  $^{22}\text{Na}$ .<sup>47</sup> At higher energies, as there is no experimental data to validate the cross section selection, and the trend of the cross-section values suggests that the contribution cannot be neglected, different assumptions have been considered. Therefore, production rates have been derived for the different assumptions in the calculation of the integral in Eq.(5). For higher energies, that means above 150-200 MeV, several options have been evaluated:

- (1) HEAD-2009<sup>48</sup> cross sections have been used, if available. It is assumed that in this high energy range neutron and proton cross sections are comparable.
- (2) The available highest energy cross-section from TENDL<sup>49</sup> has been considered as a constant value at higher energies.
- (3) The average between the available highest energy cross-section from TENDL and the corresponding results from HEAD-2009 has been considered also as a constant value at higher energies.
- (4) The average at each energy between TENDL data (and its extrapolation) and HEAD-2009 cross sections have been taken into consideration too.

In Fig. 9, for brevity sake, option (1) is referred as HEAD-2009, option (2) as TENDL extrapolation, option (3) as average extrapolation and option (4) as average.

No data have been found above 1 GeV. Although the cosmic neutron spectrum decreases quickly with energy,<sup>43</sup> cross sections seem to be still increasing with energy (see Fig. 9) and then calculations of production rates have been extended up to 10 GeV; since the particular shape of the excitation functions is difficult to predict in this energy range, a constant production cross-section from the last available energy has been assumed, giving actually a lower limit to the contribution to the production rates from neutrons of those energies.

In the range between 150 and 200 MeV there are (at least for some targets) cross sections from both TENDL and HEAD-2009. But unfortunately, there is an important mismatch between excitation functions from the two different libraries used at lower and higher energies (LE and HE, respectively), especially for iodine (see Fig. 9). This fact introduces an important uncertainty in the estimate of the production rate; to take into account and to quantify this effect, the sum between the contribution from low energy using TENDL and that from high energy considering one of the described four options has been repeated considering the cut both at 150 and at 200 MeV. Table 10 summarizes all the obtained production rates in the eight different conditions. The maximum and minimum rates define an interval, whose central value and half width have been considered as the final results and their uncertainties for the evaluation of the production rates of tritium in the different targets. For NaI, rates derived for Na and I have been properly summed.

Table 10. Production rates of  ${}^3\text{H}$  at sea level calculated for Na and I using different excitation functions.<sup>43</sup> Contributions from LE and HE have been evaluated cutting at both 150/200 MeV (see text) and summed to derive the total. The final estimated rates are given by the ranges defined between the maximum and minimum obtained rates. Results are expressed per mass unit of the NaI detector and then the production rate for NaI is the sum of Na and I values, corresponding to  $(83\pm 27) \text{ kg}^{-1}\text{d}^{-1}$ .

	Na ( $\text{kg}^{-1}\text{d}^{-1}$ )	I ( $\text{kg}^{-1}\text{d}^{-1}$ )
LE TENDL	14.3 / 18.7	15.4 / 22.9
HE(1)		14.6 / 13.6
HE(2)	14.6 / 16.6	8.7 / 55.2
HE(3)		14.2 / 29.6
HE(4)		38.6 / 34.4
total(1)		30.0 / 36.5
total(2)	28.8 / 35.2	29.6 / 78.1
total(3)		24.1 / 52.5
total(4)		54.0 / 57.3
estimated rate	$32.0 \pm 3.2$	$51 \pm 27$

It is worth noting that the actual production rates must be higher than the values reported in Table 10 since they correspond only to neutron activation. Proton activation, being much smaller, is not completely negligible. As neutron and proton fluxes are similar on the Earth surface for energies above 1 GeV, the relative contribution in the total production rate of neutrons from this very high energy range is for instance between 4 and 7% for all the analyzed targets when considering cross sections from TENDL extrapolation (situation (2)) and 10% and 13% for iodine respectively when assuming the HEAD-2009 cross sections (situation (1)). Therefore, at least a similar contribution would be expected from protons.

## 5. Comparison with other NaI(Tl) activation results

A complete study of cosmogenic activation in NaI(Tl) crystals was also performed within the DM-Ice17 experiment.<sup>34</sup> Two crystals, with a mass of 8.5 kg each and previously operated at the dark matter NaIAD experiment in the Boulby underground laboratory in UK,<sup>31</sup> were deployed at a depth of 2450 m under the ice at the geographic South Pole in December 2010 and collected data over three-and-a-half years. The activation of detector components occurred during construction, transportation, or storage at the South Pole prior to deployment. The DM-Ice17 data provided compelling evidence of significant production of cosmogenic isotopes, which was used to derive the corresponding production rates based on simulation

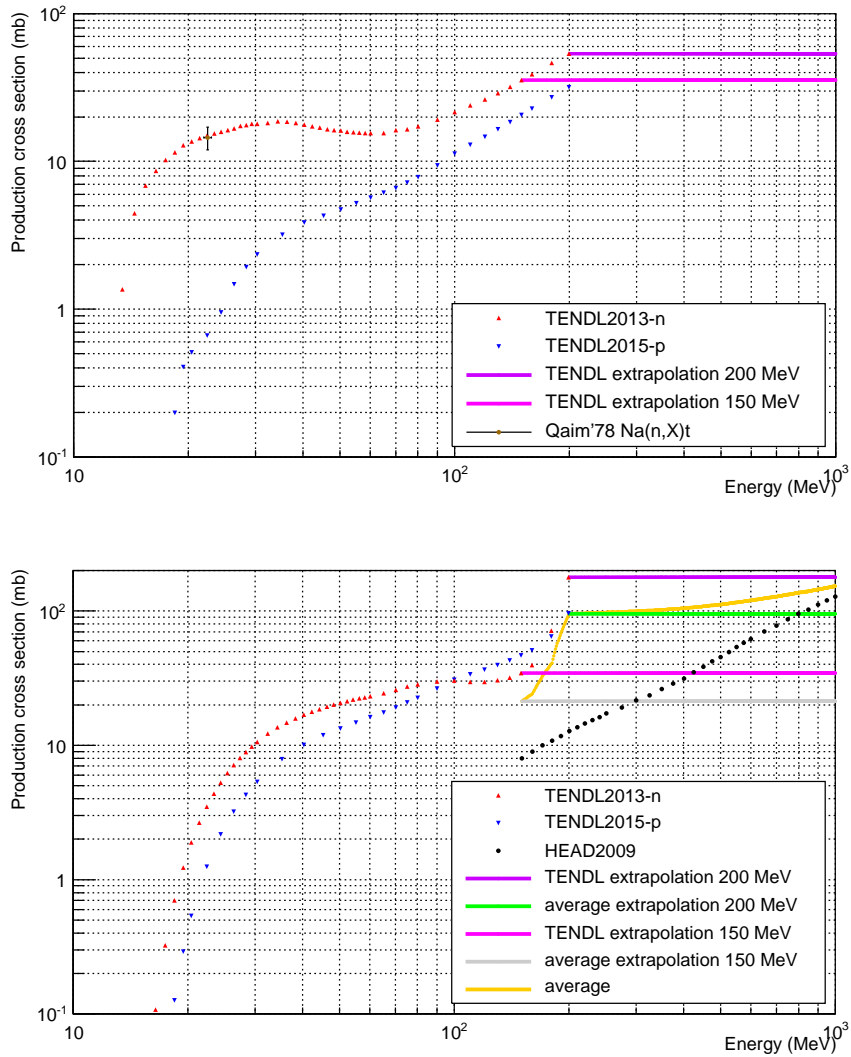


Fig. 9. Comparison of excitation functions for the production of  $^3\text{H}$  on Na (top) and I (bottom) by nucleons taken from different sources (TENDL-2013 and HEAD-2009 libraries) together with several extrapolations considered at high energies (see text).

matching. In addition, calculations based on modified ACTIVIA<sup>50</sup> using the Gordon et al. neutron spectrum<sup>46</sup> were also carried out. Results are presented in Table 11. It is worth noting that a very good agreement between measured production rates in ANAIS and DM-Ice17 crystals has been found. ACTIVIA estimates of metastable tellurium isotopes give rates clearly higher than measured values.

Table 11. Production rates (in  $\text{kg}^{-1}\text{d}^{-1}$ ) at sea level for isotopes induced in NaI(Tl) crystals following measurements by ANAIS<sup>33</sup> and DM-Ice17<sup>34</sup> experiments together with calculations based on selected excitation functions<sup>33</sup> or using the ACTIVIA code.<sup>34</sup>

Isotope	Half-life <sup>38,40</sup>	Calculation <sup>33</sup>	ANAIS measurement <sup>33</sup>	ACTIVIA <sup>34</sup>	DM-Ice17 measurement <sup>34</sup>
<sup>126</sup> I	12.93 d	297.0	283±36	128	
<sup>125</sup> I	59.407 d	242.3	220±10	221	230
<sup>124</sup> I	4.176 d	135.9			
<sup>127m</sup> Te	106.1 d	7.1	10.2±0.4	93	<9
<sup>125m</sup> Te	57.4 d	41.9	28.2±1.3	74	27
<sup>123m</sup> Te	119.3 d	33.2	31.6±1.1	52	21
<sup>123</sup> Te	>10 <sup>13</sup> y	10.2			
<sup>121m</sup> Te	164 d	23.8	23.5±0.8	93	25
<sup>121</sup> Te	19.16 d	8.4	9.9±3.7	93	
<sup>113</sup> Sn	115.09 d	9.9	6.8 ± 1.6	9.0	16
<sup>109</sup> Cd	461.9 d	1.6	2.0 ± 0.6	4.8	
<sup>22</sup> Na	2.6029 y	53.6	45.1±1.9	66	

Presence of cosmogenic isotopes has been also observed in NaI(Tl) crystals from other experiments like DAMA/LIBRA<sup>42,51,52</sup> and KIMS (now in COSINE-100).<sup>53,54</sup>

As mentioned in section 3.3, a direct identification of tritium in NaI(Tl) crystals has not been possible within the ANAIS experiment, but an estimate of the possible tritium content has been attempted. For the tritium production rate in sodium iodide, only calculations are available; results using TALYS,<sup>55</sup> GEANT4<sup>7</sup> and ACTIVIA<sup>7,55</sup> are shown in Table 12, together with the estimate based on a selection of excitation functions mainly from TENDL and HEAD-2009 libraries presented in section 4 and in Ref. 43. As it can be seen in the table, this latter rate is higher than previous estimates, but, as discussed in section 3.3, the required exposure times to get the deduced tritium activities for ANAIS detectors based on that rate roughly agree with the time lapse between sodium iodide raw material purification starting and detector shipment, according to the company.

Table 12. Production rates (in  $\text{kg}^{-1}\text{d}^{-1}$ ) of <sup>3</sup>H in sodium iodide at sea level evaluated from calculations based on different approaches (but all of them using the same neutron spectrum from Gordon et al.<sup>46</sup>).

Calculation	Rate	Reference
TALYS code	31.1	55
ACTIVIA calculation	26	34
GEANT4 code	42.9	7
ACTIVIA calculation	36.2	55
TENDL+HEAD-2009 cross sections	83±27	43

## 6. Summary and conclusions

Sodium iodide detectors are very relevant due to their properties in the search for an annual modulation effect in the dark matter interaction rates. The understanding of their backgrounds is essential and the cosmogenic activation of NaI(Tl) crystals is one of the relevant sources. In the context of the ANAIS experiment, now taking data at the Canfranc Underground Laboratory using 112.5 kg of NaI(Tl), a thorough study of cosmogenic isotopes has been made in the last years; first results for tellurium and iodine and  $^{22}\text{Na}$  were presented in Ref. 33 and the case of  $^3\text{H}$  has been specifically studied in Ref. 43. Here, all these previous results have been summarized, new estimates of cosmogenic yields for  $^{113}\text{Sn}$  and  $^{109}\text{Cd}$  have been discussed and the ANAIS results have been compared with those obtained by other experiments, finding a good agreement. Although most of the cosmogenic products in NaI(Tl) decay in acceptable times, the very low energy emissions and the longer half-lives of especially  $^{22}\text{Na}$  and  $^3\text{H}$  force to take them into consideration in the background analysis of any sodium iodide experiment devoted to dark matter searches. The implementation of cosmogenic contributions, calculated following the presented procedures, in the ANAIS background model provide a satisfactory agreement with the available experimental data.<sup>35</sup>

## Acknowledgments

This paper is dedicated to the memory of Professor J.A. Villar who passed away in August, 2017. Deeply in sorrow, we all thank his dedicated work and kindness. This work has been financially supported by the Spanish Ministerio de Economía y Competitividad and the European Regional Development Fund (MINECO- FEDER) under grants No. FPA.2011-23749 and FPA2014-55986-P; the Consolider-Ingenio 2010 Programme under grants MULTIDARK CSD2009-00064; CPAN CSD2007-00042 and the Gobierno de Aragón and the European Social Fund (Group in Nuclear and Astroparticle Physics). We also acknowledge LSC and GIFNA staff for their support.

## References

1. R. Bernabei et al., *Eur. Phys. J. C* **73**, 2648 (2013).
2. J. Amaré et al., The ANAIS-112 experiment at the Canfranc Underground Laboratory, arXiv:1710.03837.
3. I. Coarasa et al., Annual modulation of dark matter: The ANAIS-112 case, arXiv:1704.06861 [astro-ph.IM].
4. D. Lal and B. Peters, Cosmic ray produced radioactivity on the Earth, (Springer, Berlin-Heidelberg, 1967).
5. J. Beer, K. McCracken, R. von Steiger, *Cosmogenic Radionuclides. Theory and Applications in the Terrestrial and Space Environments*, (Springer, 2012).
6. S. Cebrián, *International Journal of Modern Physics A* **32**,1743006 (2017).
7. C. Zhang, D. M. Mei, V. A. Kudryavtsev, S. Fiorucci, *Astropart. Phys.* **84**, 62 (2016).

8. G. Heusser, *Annu. Rev. Nucl. Part. Sci.* **45**, 543 (1995).
9. J. A. Formaggio and C. J. Martoff, *Annu. Rev. Nucl. Part. Sci.* **54**, 361 (2004).
10. P. Gondolo, *Nuclear Data Sheet* **120**, 175 (2014).
11. V. Kudryavtsev, *Presentation at Low Radioactivity Techniques 2017 workshop*, Seoul, Korea, <http://indico.ibs.re.kr/event/46/session/7/contribution/20>.
12. A. F. Barghouty et al., *Nucl. Instrum. Meth. B* **295**, 16 (2013).
13. V. Lozza and J. Petzoldt, *Astropart. Phys.* **61**, 62 (2015).
14. B.S. Wang et al., *Phys. Rev. C* **92**, 24620 (2015).
15. L. Baudis et al., *Eur. Phys. J. C* **75**, 485 (2015).
16. C. Zhang et al., *Astropart. Phys.* **84**, 62 (2014).
17. O. Lebeda et al., *Phys. Rev. C* **85**, 014602 (2012).
18. O. Lebeda et al., *Nucl. Phys. A* **929**, 129 (2014).
19. S. Cebrián et al., *Astropart. Phys.* **33**, 316 (2010).
20. M. Laubenstein, G. Heusser, *App. Rad. Isot.* **67**, 750 (2009).
21. I. Coarasa et al., *Journal of Physics: Conference Series* **718** 042049 (2016).
22. V.E. Guiseppe et al., *Astropart. Phys.* **64**, 34 (2015).
23. Decay Data Evaluation Project, [http://www.nucleide.org/DDEP\\_WG/Nuclides/H-3\\_tables.pdf](http://www.nucleide.org/DDEP_WG/Nuclides/H-3_tables.pdf).
24. K. Fushimi et al., *Phys. Rev. C* **47**, 425 (1993).
25. K. Fushimi et al., *Astropart. Phys.* **12**, 185 (1999).
26. M.L. Sarsa et al., *Phys. Lett. B* **386**, 458 (1996).
27. M.L.Sarsa et al., *Phys. Rev. D* **56**, 1856 (1997).
28. R. Bernabei et al., *Phys. Lett. B* **450**, 448 (1999).
29. R. Bernabei et al., *Riv. Nuovo Cim. A* **112**, 545 (1999).
30. G. Gerbier et al., *Astropart. Phys.* **11**, 287 (1999).
31. G.J. Alner et al., *Phys. Lett. B* **616**, 17 (2005).
32. K. Fushimi et al., *J. Phys.: Conf. Ser.* **469**, 012011 (2013).
33. J. Amaré et al., *Journal of Cosmology and Astroparticle Physics* **02**, 046 (2015).
34. W. C. Pettus, Ph.D. thesis, University of Wisconsin-Madison (2015).
35. J. Amaré et al., *Eur. Phys. J. C* **76**, 429 (2016).
36. S. Cebrián et al., *Astropart. Phys.* **37**, 60 (2012).
37. M. A. Oliván et al., *Astropart. Phys.* **93**, 86 (2017).
38. <http://www.nucleide.org/DDEP.htm>
39. S. Ohya, *Nucl. Data Sheets* **111**, 1619 (2010).
40. WWW Table of Radioactive Isotopes, <http://ie.lbl.gov/toi/>.
41. J. F. Ziegler, *IBM J. Res. Develop.* **42**, 117 (1998).
42. R. Bernabei et al., *Nucl. Instrum. Meth. A* **592**, 297 (2008).
43. J. Amaré et al., *Astropart. Phys.* **97**, 96 (2018).
44. P. Villar, Background evaluation of the ANAIS dark matter experiment in different configurations: towards a final design, PhD Dissertation, Universidad de Zaragoza, 2016, <https://zaguan.unizar.es/record/58561/files/TESIS-2017-007.pdf>.
45. R. C. Reedy, *Nucl. Instrum. Meth. B* **294**, 470 (2013).
46. M. S. Gordon et al., *IEEE Transactions on Nuclear Science* **51**, 3427 (2004). Erratum: M. S. Gordon et al., *IEEE Transactions on Nuclear Science* **52**, 2703 (2005).
47. S. M. Qaim and R. Wölflé, *Nuclear Physics A* **295(1)**, 150 (1978).
48. Y.A. Korovin, *Nucl. Instrum. Meth. A* **624**, 20 (2010).
49. A.J. Koning, D. Rochman, *Nuclear Data Sheets* **113**, 2841 (2012).
50. J. J. Back and Y. A. Ramachers, *Nucl. Instrum. Meth. A* **586**, 286 (2008).
51. R. Bernabei et al., *Int. J. Mod. Phys. A* **31**, 1642002 (2016).
52. R. Bernabei and A. Incicchitti, *International Journal of Modern Physics A* **32**, 1743007

*Study of the cosmogenic activation in NaI(Tl) crystals within the ANAIS experiment* 31

(2017).

53. P. Adhikari et al., *Eur. Phys. J. C* **76**, 185 (2016).
54. G. Adhikari et al., *Eur. Phys. J. C* **77**, 437 (2017).
55. D. M. Mei et al., *Astropart. Phys.* **31**, 417 (2009).